Research Article

Hloniphile M. Sithole, Sabyasachi Mondal*, Precious Sibanda, and Sandile S. Motsa

An unsteady MHD Maxwell nanofluid flow with convective boundary conditions using spectral local linearization method

https://doi.org/10.1515/phys-2017-0074
Received Jan 30, 2017; accepted Jul 03, 2017

Abstract: The main focus of this study is on unsteady Maxwell nanofluid flow over a shrinking surface with convective and slip boundary conditions. The objective is to give an evaluation of the impact and significance of Brownian motion and thermophoresis when the nanofluid particle volume fraction flux at the boundary is zero. The transformed equations are solved numerically using the spectral local linearization method. We present an analysis of the residual errors to show the accuracy and convergence of the spectral local linearization method. We explore the effect of magnetic field and thermophoresis parameters on the heat transfer rate. We show, among other results, that an increase in particle Brownian motion leads to a decrease in the concentration profiles but concentration profiles increase with the increasing value of thermophoresis parameter

Keywords: Unsteady Maxwell nanofluid; Navier slip; Ohmic dissipation; Spectral local linearization method

PACS: 47.11.Kb

1 Introduction

There have been only a few studies on Maxwell nanofluid flow for a shrinking sheet in the recent past. However, in general, research on non-Newtonian fluid flow has gained sizeable attention because of the multiplicity of its applications in the biomedical and chemical industries [1]. A non-Newtonian fluid is a fluid whose viscosity varies with the applied stress. The relation between the strain rate and the shear stress is nonlinear, and can be time-dependent [2]. The constitutive equations tend to be highly nonlinear and intricate in comparison with those of a Newtonian fluid. A Maxwell fluid is a viscoelastic material having the properties of elasticity and viscosity [3]. Unlike the Newtonian model, the upper convected Maxwell (UCM) model incorporates relaxation time.

The UCM model has been studied by many researchers, for example, Choi *et al.* [4] gave an analysis of incompressible steady two-dimensional UCM fluid flow in a porous channel. Their study included a consideration of inertia and fluid elasticity. Nandy [5] focused on the unsteady boundary layer flow of a Maxwell nanofluid over a permeable shrinking sheet with a Navier slip condition at the surface. The flow equations were solved using the shooting method. The homotopy analysis method was used by Rashidi *et al.* [6] to find solutions to the conservation equations for heat and mass transfer in a two-dimensional steady magnetohydrodynamic fluid flow in a porous medium [6]. Awais [7] investigated heat absorption and generation in steady flow over a surface stretched linearly in its own plane using the UCM fluid model. A nanofluid is defined as a fluid with suspended solid nanoparticles that are less than $100nm$ in size, and solid volume fraction less than 4%, [8]. Even at low nanoparticle volume concentration, nanofluids have been shown to have improved conductivity and thermal the performance compared to base fluids such as water and oil, [9].

The unsteady Maxwell fluid flow over a stretching surface subject to constructive/destructive chemical reaction was studied by Mukhopadhyay and Bhattacharyya [10].

***Corresponding Author: Sabyasachi Mondal:** Past address: School of Mathematics, Statistics and Computer Science, University of KwaZulu-Natal, Pietermaritzburg-3209, South Africa;
Present address: Amity University, Kolkata-700135, West Bengal, India;
Email: sabya.mondal.2007@gmail.com
Hloniphile M. Sithole: School of Mathematics, Statistics and Computer Science, University of KwaZulu-Natal, Pietermaritzburg-3209, South Africa
Precious Sibanda: School of Mathematics, Statistics and Computer Science, University of KwaZulu-Natal, Pietermaritzburg-3209, South Africa
Sandile S. Motsa: School of Mathematics, Statistics and Computer Science, University of KwaZulu-Natal, Pietermaritzburg-3209, South Africa

They showed that for a constructive chemical reaction the concentration field increased but decreased for a destructive chemical reaction [10]. Also, in line with physical expectations, the concentration boundary-layer decreased for a destructive chemical reaction. Nandy *et al.* [11] studied forced convection in an unsteady nanofluid flow past a permeable shrinking sheet subject to heat loss due to thermal radiation. They explored the simultaneous impact of a magnetic field, thermal radiation, and unsteadiness on the heat transfer and flow properties of the fluid. Das *et al.* [12] presented simulated results for heat and mass transfer in an electrically conducting incompressible nanofluid flow near a heated stretching sheet with a convective boundary condition. The impact of an inclined magnetic field in the flow of a fluid with variable thermal conductivity was studied by Hayat et al. [13, 14]. An analysis of the significance of a heat source/ sink and temperature dependent thermal conductivity was given. Qasim and Hayat [15] investigated the impact of heat loss through thermal radiation in unsteady magnetohydrodynamic flow of a micropolar fluid. The influence of Joule heating and thermophoresis in a Maxwell fluid was studied in [16].

Som *et al.* [17] studied Ohmic dissipation and thermal radiation in flow over a stretching sheet embedded in a porous media. The results indicated that fluid injection causes a reduction in heat transfer whereas fluid suction raises the heat transfer coefficient. Hsiao [18] studied conjugate heat transfer with Ohmic dissipation in an incompressible Maxwell fluid close to a stagnation point. Mahapatra *et al.* [19] gave an analysis of stagnation point fluid flow over a stretching surface.

The purpose of this study is to investigate unsteady two-dimensional boundary-layer flow, heat and mass transfer in a Maxwell nanofluid flow over shrinking sheet with both slip and convective boundary conditions. The objective is to extend the study by Nandy [5] to include an evaluation of the impact and significance of thermophoresis and Brownian motion when the nanofluid particle volume fraction at the boundary is not actively controlled. The conservation equations are solved numerically using the spectral local linearization method, see Motsa [20, 21]. To show the accuracy of the numerical scheme, analysis of the residual errors is given for different physical parameter values. The effect of several physical parameters on the fluid properties are shown in tabular and graphical form. Comparison with published work for special cases shows an excellent agreement.

2 Problem formulations

An unsteady laminar boundary layer flow of an incompressible viscous Maxwell nanofluid over a shrinking surface in two dimensions is considered here. The shrinking sheet velocity is $u_w(x, t)$ while the mass transfer velocity is $v_w(x, t)$, t denotes time and x is measured along the sheet. Using the nanofluid model proposed by Buongiorno [22], the conservation equations for mass, momentum, thermal energy and nanoparticles for a Maxwell fluid are:

$$\frac{\partial u}{\partial x} + \frac{\partial v}{\partial y} = 0, \tag{1}$$

$$\begin{aligned}\frac{\partial u}{\partial t} + u\frac{\partial u}{\partial x} + v\frac{\partial u}{\partial y} = \nu\frac{\partial^2 u}{\partial y^2} - k_0\left(u^2\frac{\partial^2 u}{\partial x^2}\right. \\ \left. +2uv\frac{\partial^2 u}{\partial x\partial y} + v^2\frac{\partial^2 u}{\partial y^2}\right) \\ - \frac{\sigma B^2}{\rho_f}\left(u - kv\frac{\partial u}{\partial y}\right),\end{aligned} \tag{2}$$

$$\begin{aligned}&\frac{\partial T}{\partial t} + v\frac{\partial T}{\partial y} + u\frac{\partial T}{\partial x} = \alpha\frac{\partial^2 T}{\partial y^2} \\ &+ \frac{1}{\rho_f c_p}\frac{\partial}{\partial y}\left[\kappa(T)\frac{\partial T}{\partial y}\right] \\ &+ \frac{\mu}{\rho_f c_p}\left(\frac{\partial u}{\partial y}\right)^2 + \frac{\sigma}{\rho_f c_p}(uB_0 - E_0)^2 + \frac{Q_0}{\rho_f c_p}(T - T_\infty) \\ &+ \left[\tau D_B\frac{\partial C}{\partial y}\frac{\partial T}{\partial y} + \frac{\tau D_T}{T_\infty}\left(\frac{\partial T}{\partial y}\right)^2\right] + \frac{D_m k_0}{c_s c_p}\frac{\partial^2 C}{\partial y^2} \\ &- \frac{1}{\rho_f c_p}\frac{\partial q_r}{\partial y},\end{aligned} \tag{3}$$

$$\begin{aligned}\frac{\partial C}{\partial t} + v\frac{\partial C}{\partial y} + u\frac{\partial C}{\partial x} = D_B\frac{\partial^2 C}{\partial y^2} + \frac{D_T}{T_\infty}\frac{\partial^2 T}{\partial y^2} \\ + \frac{D_m k_0}{T_m}\frac{\partial^2 T}{\partial y^2} - k_1(C - C_\infty),\end{aligned} \tag{4}$$

where u is the velocity component in the x- direction and v is the velocity component in the y-direction. The kinematic viscosity is ν, the relaxation time of the UCM fluid is k_0, the thermal diffusivity is α, the variable thermal conductivity is $\kappa(T)$ and the chemical reaction parameter is k_1. The Brownian diffusion coefficient is D_B, while the thermophoresis diffusion coefficients is D_T. Here, τ is the effective heat capacity of the nanoparticle material divided by the heat capacity of the ordinary fluid, T is the fluid temperature and C is the nanoparticle volume fraction. The temperature and the nanoparticle concentration at the wall are T_w and C_w, respectively, and T_∞ and C_∞ denote the ambient temperature and concentration respectively.

The velocity slip is proportional to the local shear stress. These equations are subject to the boundary conditions:

$$\begin{aligned} &u = u_w(x,t) + u_{\text{slip}}(x,t),\ v = v_w(x,t), \\ &-k_0\sqrt{1-\lambda t}\frac{\partial T}{\partial y} = h_f(T_w - T), \\ &D_B\frac{\partial C}{\partial y} + \frac{D_B}{T_\infty}\frac{\partial T}{\partial y} = 0 \text{ at } y = 0, \\ &u \to 0, T \to T_\infty, \frac{\partial u}{\partial y} \to 0, C \to C_\infty \text{as} y \to \infty, \end{aligned} \tag{5}$$

where $k_0 = k(1-\lambda t)$, $u_w(x,t) = -ax(1-\lambda t)^{-1}$, $u_{\text{slip}}(x,t) = vN_1\partial u/\partial y$, $N_1 = N\sqrt{1-\lambda t}$ is the slip velocity , λ is the unsteadiness parameter and $k_0(>0)$, $a(>0)$ are positive constants. This assumption is to allow for the possibility of a similarity solution. We introduce the similarity variables:

$$\begin{aligned} &\eta = y\sqrt{\frac{a}{v(1-\lambda t)}}, \quad \psi = \sqrt{\frac{av}{1-\lambda t}}xf(\eta), \\ &T(x,t) = T_\infty + \theta(\eta)(T_w - T_\infty), \\ &C(x,t) = C_\infty + \phi(\eta)(C_w - C_\infty), \end{aligned} \tag{6}$$

where ψ is the stream function, defined by $v = -\partial\psi/\partial x$ and $u = \partial\psi/\partial y$. Equations (1) - (4) are transformed to

$$\begin{aligned} &f''' - f'^2 + ff'' - A\left(\frac{\eta}{2}f'' + f'\right) \\ &-\beta\left(f^2f''' - 2ff'f''\right) - M^2f' - M^2\beta ff'' = 0, \end{aligned} \tag{7}$$

$$\begin{aligned} &\frac{1}{Pr_{eff}}\theta'' + \frac{1}{Pr}\left[\theta''(1+\varepsilon\theta) + \varepsilon\theta'^2\right] + E_cf''^2 \\ &+ E_cM^2\left(f' - E_1\right)^2 + \left(f - A\frac{\eta}{2}\right)\theta' \\ &+ D_f\phi'' + He\theta + Nt\theta'^2 + Nb\theta'\phi' = 0, \end{aligned} \tag{8}$$

$$\begin{aligned} &\phi'' + S_c\left(f - A\frac{\eta}{2}\right)\phi' + \frac{Nt}{Nb}\theta'' - \gamma S_c\phi + \frac{Nt}{Nb}\theta'' \\ &+ S_cS_r\theta'' = 0, \end{aligned} \tag{9}$$

where the prime denotes derivatives with respect to η. The boundary conditions are

$$\begin{aligned} &f'(0) = -1 + \delta f''(0), f(0) = s, f''(\infty) = 0, f'(\infty) = 0, \\ &\theta'(0) = -B_i(-\theta(0) + 1), \theta(\infty) = 0, \\ &Nb\phi'(0) + Nt\theta'(0) = 0, \phi(\infty) = 0, \end{aligned} \tag{10}$$

where the parameter $\delta = N\sqrt{av}$ is the non-dimensional velocity slip and $v_w(0,t)$ is the wall mass transfer velocity given by

$$v_w(0,y) = \frac{v_0}{\sqrt{1-\lambda t}},$$

where v_0 is the constant mass flux velocity. Thus

$$s = -\frac{v_0}{av} = f(0),$$

where wall mass suction occurs when $s > 0$ while wall mass injection occurs when $s < 0$. The non-dimensional parameters in the above equations are the Maxwell parameter $\beta(= k_0a)$, the unsteadiness parameter $A\left(= \lambda/a\right)$, the magnetic field parameter $M\left(= \sqrt{\sigma B_0^2/\rho_f a}\right)$, $He\left(= Q_0/\rho_f c_p\right)$ the heat generation parameter and $Q(= Q_0(1-\lambda t))$, $Nb\left(= \tau D_B(C_w - C_\infty)/v\right)$ is the Brownian motion parameter and $Nt\left(= \tau D_T(T_w - T_\infty)/vT_\infty\right)$ is the thermophoresis parameter. The Prandtl number is $Pr\left(= v/\alpha\right)$, the Schmidt number is $Sc\left(= v/D_B\right)$, $Pr_{eff}\left(= Pr/(1+\frac{4}{3}R)\right)$ is the effective Prandtl number, $B_i\left(= h_f/k_0\sqrt{\frac{v}{a}}\right)$ is the Biot number, $\gamma = k_1(C_w - C_\infty)$ is the reaction parameter where $\gamma < 0$ denotes a destructive reaction, $\gamma = 0$ indicates that there is no reaction and $\gamma > 0$ denotes a generative reaction.

Other important physical parameters are the variable thermal conductivity $\kappa(T)$, the Eckert number E_c, the local electromagnetic parameter E_1, the Soret number S_r, the Dufour number D_f and the radiation parameter R. These are defined as

$$\begin{aligned} &\kappa(T) = K_\infty\left(1 + \varepsilon\frac{T - T_\infty}{\Delta T}\right), E_c = \left(\frac{x^2a^2}{c_p\Delta T(1-\lambda t)}\right), \\ &E_1 = \left(\frac{E_0(1-\lambda t)}{aB_ox}\right), \end{aligned} \tag{11}$$

$$\begin{aligned} &S_r = \left(\frac{D_mk_0\Delta T}{T_mv\Delta C}\right), D_f = \left(\frac{D_mk_0\Delta C}{c_sc_p\Delta T}\right), \\ &R = \frac{4\sigma_1T_\infty^3}{K_1\rho_fc_p\alpha_m}, \end{aligned} \tag{12}$$

where ε is a small parameter, $\Delta T = T_w - T_\infty$ and the thermal conductivity parameter is K_∞. The important flow attributes, the Nusselt number Nu_x and skin friction coefficient C_f are described by

$$C_f = \frac{\tau_w}{\rho u_w^2(x)}, \quad Nu_x = \frac{xq_w}{k(T_f - T_\infty)}. \tag{13}$$

Here q_w and τ_w are the plate heat flux and the skin friction respectively, defined as

$$q_w = -k\left(\frac{\partial T}{\partial y}\right)_{y=0}, \ \tau_w = \mu\left(\frac{\partial u}{\partial y}\right)_{y=0}, \tag{14}$$

where μ is the coefficient of viscosity. Equations (13) may be written as

$$Re_x^{\frac{1}{2}}C_f = f''(0), \tag{15}$$

$$Re_x^{-\frac{1}{2}}Nu_x = -\theta'(0), \tag{16}$$

where $Re_x = \frac{u_w(x)x}{v}$ is the local Reynolds number. Here, the Sherwood number is zero, due to the assumption of zero mass flux at the surface.

3 Method of solution

The transport equations have been solved using the iterative spectral local linearization method (SLLM), see Motsa [20]. In principle of the SLLM algorithm is to linearize and decouple the system of equations. Motsa *et al.* [21] used the spectral local linearization method to solve the equations that model natural convection in glass-fibre production processes. Shateyi and Marewo [23] used the SLLM to solve equations that models an unsteady MHD flow and heat transfer. Nonetheless, this method has only been used in a limited number of studies, hence its general validation in complex systems remains to be made. For the interested reader, the SLLM algorithm is described in [20].

The differential equations arising from the linearization procedure are solved using a Chebyshev pseudo spectral method. The domain of the problem is transformed to the interval $[-1, 1]$ using the transformation $(b - a)(\tau + 1)/2$. The differentiation matrix D is used to approximate the derivatives $Z_i(\eta)$ of the unknown variables to the matrix vector product,

$$\frac{dZ_i}{d\eta} = \sum_{k=0}^{\bar{N}} \boldsymbol{D}_{lk} Z_i(\tau_k) = \boldsymbol{D}\boldsymbol{Z}_{\boldsymbol{i}}, \quad l = 0, 1, \ldots, \bar{N}, \tag{17}$$

where the vector function at the collocation points is given by $Z = [z(\tau_0), z(\tau_1), \ldots, z(\tau_N)]^T$, $\boldsymbol{D} = 2D/(b-a)$ with $\bar{N}+1$ collocation points, [20] and

$$Z_j^{(p)} = \boldsymbol{D}^p \boldsymbol{Z}_j. \tag{18}$$

where the superscript in $\boldsymbol{D}$ denotes higher order derivatives.

SLLM Algorithm

The differential equations (7) - (9) may collectively be stated as,

$$\omega_k[F, T, H] = 0, \qquad \text{for} \qquad k = 1, 2, 3 \tag{19}$$

where ω_1, ω_2 and ω_3 are non-linear operators and F,H, T are given by

$$F = \left\{ f, \frac{\partial f}{\partial \eta}, \frac{\partial^2 f}{\partial \eta^2}, \frac{\partial^3 f}{\partial \eta^3} \right\}, \tag{20}$$

$$T = \left\{ \theta, \frac{\partial \theta}{\partial \eta}, \frac{\partial^2 \theta}{\partial \eta^2} \right\}, \tag{21}$$

$$H = \left\{ \phi, \frac{\partial \phi}{\partial \eta}, \frac{\partial^2 \phi}{\partial \eta^2} \right\}. \tag{22}$$

The system of equations (19) can be simplified and decoupled by linearizing the nonlinear terms. The Chebychev pseudo-spectral collocation method is utilized to integrate the decoupled system. The simple algorithm is as follows:

1. From the first equation, find F while treating H and T as known functions from initial guesses. This gives F_{r+1}
2. Solve for T in the second equation while treating F and H as known functions, T is known from 1 above and H is known from the initial guess. This gives T_{r+1}
3. Finally, solve for H in the last equation while treating F and T as known functions, T and H are known from 1 and 2 above. We obtain T_{r+1}.
4. Repeat steps 1-3 to find the next iterative solutions.

Using these ideas the nonlinear system of equations (7) - (9) are written as:

$$\begin{aligned} &a_{1,r} f'''_{r+1} + a_{2,r} f''_{r+1} + a_{3,r} f'_{r+1} \\ &\quad + a_{4,r} f_{r+1} = a_{5,r}, \\ &b_{1,r}\theta''_{r+1} + b_{2,r}\theta'_{r+1} + b_{3,r}\theta_{r+1} = b_{4,r}, \\ &c_{1,r}\phi''_{r+1} + c_{2,r}\phi'_{r+1} + c_{3,r}\phi_{r+1} = c_{4,r}, \end{aligned} \tag{23}$$

subject to boundary conditions:

$$\begin{aligned} &f_{r+1}(0) = s, f'_{r+1}(0) \\ &\quad = -1 + \delta f''_{r+1}(0), f''_{r+1}(\infty) = 0, \\ &f'_{r+1}(\infty) = 0, \\ &\theta'_{r+1}(0) = -B_i(1 - \theta_{r+1}(0)),\ \theta_{r+1}(\infty) = 0, \\ &Nb\phi'_{r+1}(0) + Nt\theta'_{r+1}(0) = 0,\ \phi_{r+1}(\infty) = 0. \end{aligned} \tag{24}$$

where

$$\begin{aligned} a_{1,r} &= 1 - \beta f_r^2, a_{2,r} \\ &= f_r + 2\beta f_r f'_r - A\frac{\eta}{2} - M^2 \beta f_r, \\ a_{3,r} &= 2\beta f_r f''_r - 2f'_r - A - M^2, \\ a_{4,r} &= f''_r - 2\beta f_r f'''_r + 2\beta f'_r f''_r - M^2 \beta f''_r, \\ a_{5,r} &= f_r f''_r - f'^2_r - 2\beta f_r^2 f'''_r + 4\beta f_r f'_r f''_r \\ &\quad - M^2 \beta f_r f''_r, \end{aligned} \tag{25}$$

$$\begin{aligned} b_{1,r} &= \frac{\epsilon}{Pr}\theta_r + \frac{1}{Pr_{eff}} + \frac{1}{Pr}, \\ b_{2,r} &= \frac{2\epsilon}{Pr}\theta'_r + f_r + Nb\phi'_r + 2Nt\theta'_r - A\frac{\eta}{2}, \\ b_{3,r} &= \frac{\epsilon}{Pr}\theta''_r, b_{4,r} = He, b_{5,r} = \frac{\epsilon}{Pr}\theta''_r\theta_r + \frac{\epsilon}{Pr}\theta'^2_r \\ &\quad - E_c f''_r - E_c M^2 \left(f'_r - E_1\right)^2 - D_f \phi'_r - Nt\theta'^2_r, \\ c_{1,r} &= S_c f_r - S_c A\frac{\eta}{2}, c_{2,r} = -\gamma S_c, \\ c_{3,r} &= -S_c S_r \theta''_r - \frac{Nt}{Nb}\theta''_r. \end{aligned} \tag{26}$$

Table 1: Comparison of the skin friction coefficient and Nusselt number between the results of present study and reported by Hayat *et al.* [24] when $\beta = 0.2$, $\alpha = 0.3$, $Pr = 1$, $s = 0.5$ and the other parameters are set to zero

Iterations	[24] $-f''(0)$	Current study $-f''(0)$	[24] $-\theta'(0)$	Current study $-\theta'(0)$
1	0.2829900	0.28139017	0.4300000	0.40401296
2	-	0.28149501	-	0.40465707
3	-	0.28149504	-	0.40465726
4	-	0.28149505	-	0.40465726
5	0.2814982	0.28149505	0.4064811	0.40465726
6	-	0.28149505	-	0.40465726
7	-	0.28149505	-	0.40465726
8	-	0.28149505	-	0.40465726
9	-	0.28149505	-	0.40465726
10	0.2814950	0.28149505	0.4047923	0.40465726
20	0.2814950	0.28149505	0.4046587	0.40465726
35	0.2814950	0.28149505	0.4046572	0.40465726
40	0.2814950	0.28149505	0.4046572	0.40465726

The following decoupled matrix system of equations is obtained:

$$\begin{aligned} \mathbf{A}_1\mathbf{F}_{r+1} &= \mathbf{B}_1 \\ \mathbf{A}_2\mathbf{T}_{r+1} &= \mathbf{B}_2 \\ \mathbf{A}_3\mathbf{H}_{r+1} &= \mathbf{B}_3 \end{aligned} \tag{27}$$

with corresponding boundary conditions

$$\begin{aligned} &f_{r+1}(\tau_N) = s, f'_{r+1}(\tau_N) = -1 + \delta f''_{r+1}(\tau_N), \\ &f''_{r+1}(\tau_0) = 0, f'_{r+1}(\tau_0) = 0, \\ &\theta'_{r+1}(\tau_N) = -B_i(1 - \theta_{r+1}(\tau_N)), \theta_{r+1}(\tau_0) = 0, \\ &Nb\phi'_{r+1}(\tau_N) + Nt\theta'_{r+1}(\tau_N) = 0, \phi_{r+1}(\tau_0) = 0. \end{aligned} \tag{28}$$

where

$$\begin{aligned} \mathbf{A}_1 &= \mathbf{diag}\,[\mathbf{a}_{1,r}]\,\mathbf{D}^3 + \mathbf{diag}\,[\mathbf{a}_{2,r}]\,\mathbf{D}^2 \\ &+ \mathbf{diag}\,[\mathbf{a}_{3,r}]\,\mathbf{D} + \mathbf{diag}\,[\mathbf{a}_{4,r}]\,, \mathbf{A}_1 = \mathbf{a}_{5,r} \\ \mathbf{A}_2 &= \mathbf{diag}\,[\mathbf{b}_{1,r}]\,\mathbf{D}^2 + \mathbf{diag}\,[\mathbf{b}_{2,r}]\,\mathbf{D} + \mathbf{diag}\,[\mathbf{b}_{3,r}] \\ &+ \mathbf{b}_{4,r}\mathbf{I}, \mathbf{A}_2 = \mathbf{c}_{5,r} \\ \mathbf{A}_3 &= \mathbf{D}^2 + \mathbf{diag}\,[\mathbf{c}_{1,r}]\,\mathbf{D} + \mathbf{c}_{2,r}\mathbf{I}, \quad \mathbf{A}_3 = \mathbf{c}_{3,r}. \end{aligned} \tag{29}$$

$\mathbf{I}$ is an identity matrix with $(\bar{N}+1)$ rows and columns, $\mathbf{F}$, $\mathbf{H}$ and $\mathbf{T}$ are approximate values of f, ϕ and θ calculated at the collocation points. Initial approximations are required to start the iteration process, and these can be selected so as to satisfy the boundary conditions and known flow configuration. For our system, the following guesses were used as suitable initial approximations,

$$f_0(\eta) = \frac{\alpha}{1+\delta}(-e^{-\eta} + 1) + s, g_0(\eta) \tag{30}$$

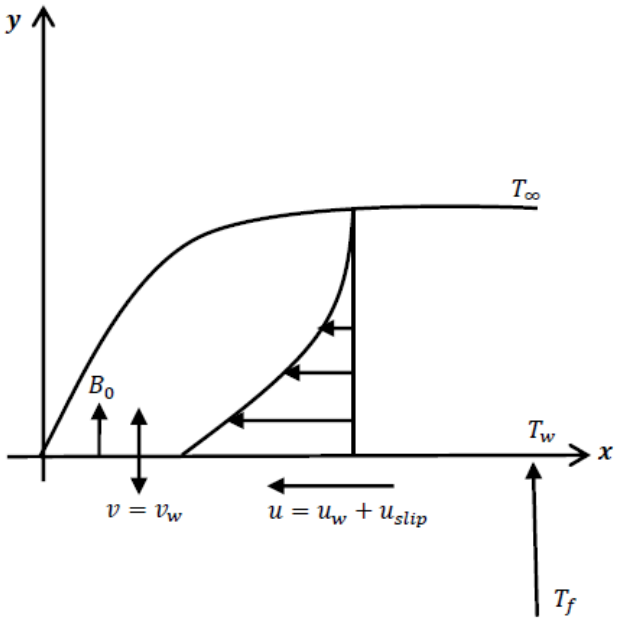

Figure 1: Flow geometry of the problem

$$= \frac{B_i}{1+B_i}e^{-\eta},$$

$$\theta_0(\eta) = \frac{N_t B_i}{N_b(1+B_i)}e^{-\eta}.$$

The boundary conditions are inserted in the matrices in (27) and the approximate solutions at each iteration level are obtained by solving (27).

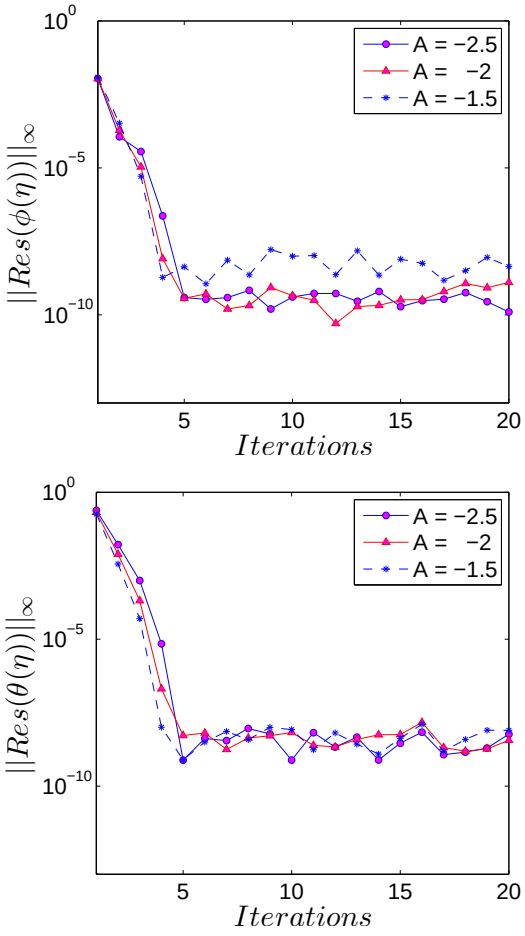

Figure 2: Residual errors for θ and ϕ when $A = -2.5, -2.0, -1.5$

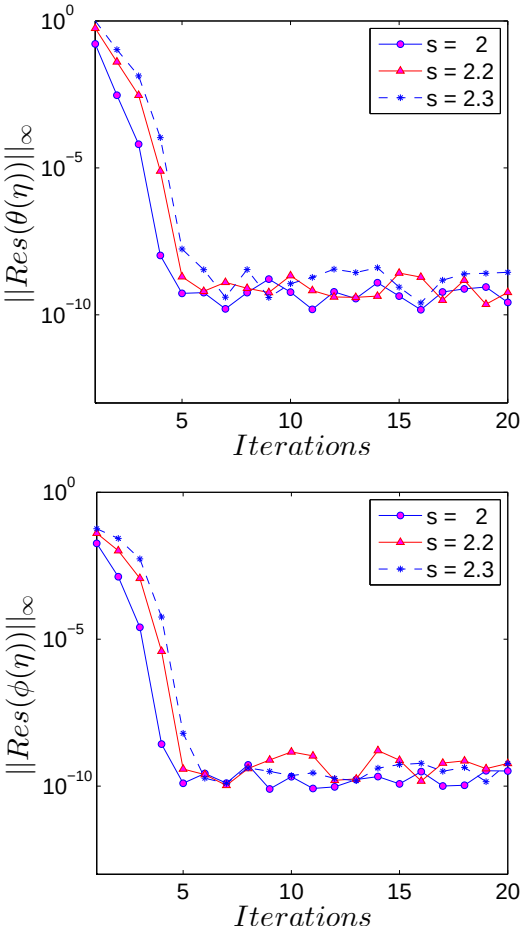

Figure 3: Residual errors for θ and ϕ when $s = 2, 2.2, 2.3$

Table 2: Computed values of the Nusselt number for different values of Nb, M and Nt

Nb	M	Nt	$\lvert-\theta'(0)\rvert$
0.2			0.06758610
0.4	0.3	0.1	0.06758600
0.8			0.06758579
	0.1		0.09046540
0.2	0.3	0.1	0.08959087
	0.5		0.08728149
		0.05	0.08031901
0.2	0.3	0.07	0.08434208
		0.10	0.09125982

4 Results and discussion

The solutions of the differential equations are given Tables 1 - 2 and Figures 2 - 16. In Table 1 we establish the reliability of the numerical scheme by a comparative analysis of the skin friction coefficient C_f and Nusselt number Nu_x with results reported by Hayat et al. [24] when $\beta = 0.2$, $\alpha = 0.3$, $Pr = 1$ and $s = 0.5$. The other parameters have been set to zero. A good agreement is observed with the previously published work. To gain further insights as to the accuracy and convergence of the method used in this study, we have calculated residual errors as shown in Figures 2 to 4. These are calculated for different values of A, s and β. In general, the solutions have converged with an absolute residual error $||\text{Res}|| \approx 10^{-11}$ after five iterations. These results sufficiently demonstrate to the accuracy and convergence of the SLLM.

The numerical computations have been done when $A = -1.0, s = 2, \delta = 0.25, Nb = Nt = 0.1, Sc = 0.8, Pr = 1.0, M = 0.3, \varepsilon = 0.1, E_c = 0.1, E_1 = 1.0, D_f = 0.1, He = 0.5, Sr = 0.1, Pr_{eff} = 1.0, \gamma = 0.1$, and $Bi = 0.1$. For numerical simulations, the parameter values are chosen from the previous literature on nanofluid flow such as [5, 10, 12, 16, 24] etc. Table 2 shows the Nusselt number for different Nb, M and Nt, the other parameters as stated above. The results show that Nu_x decreases with increas-

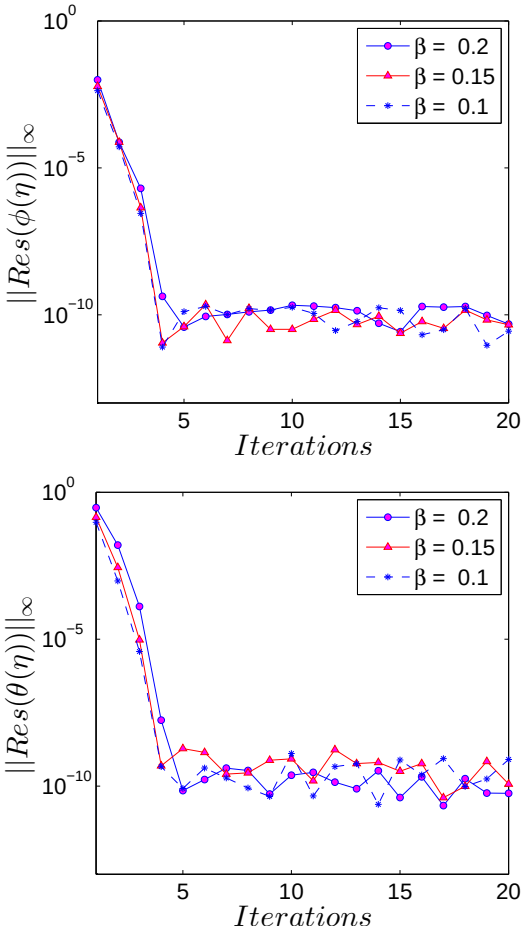

Figure 4: Residual errors for θ and ϕ when $\beta = 0.1, 0.15, 0.2$

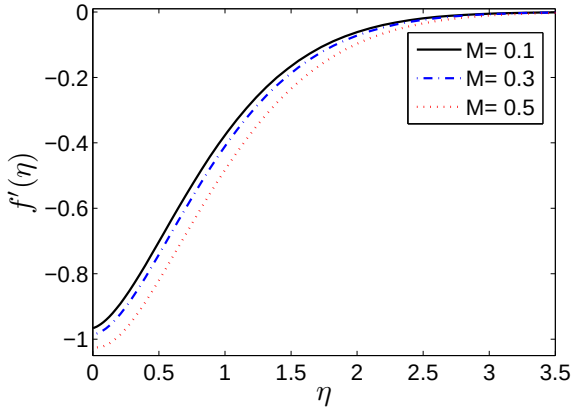

Figure 5: Effect of magnetic field parameter M on the velocity profile $f'(\eta)$

ing Nb and M whereas the opposite is observed for increasing values of Nt.

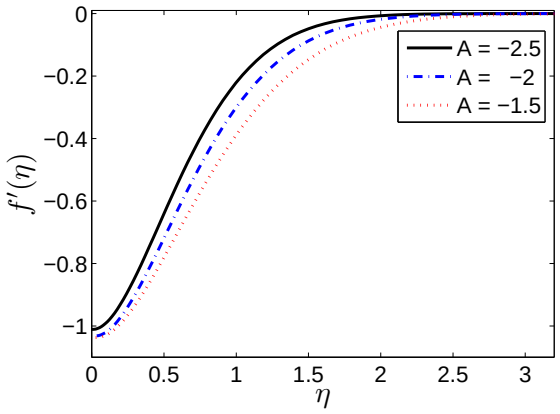

Figure 6: Effect of A on the velocity profile $f'(\eta)$

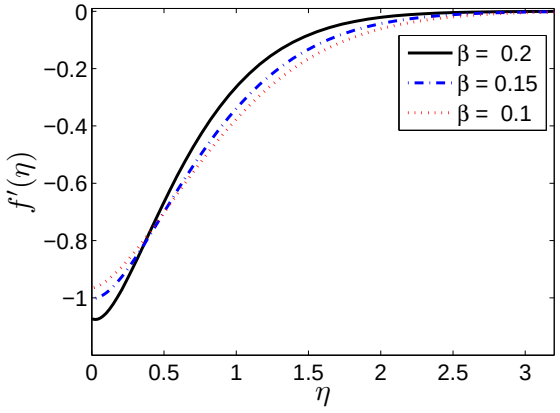

Figure 7: Effect of β on the velocity profile $f'(\eta)$

Figure 5 shows that the velocity reduces with increasing magnetic field strength. This is an indication of an increase in the Lorentz force that creates a resistance to the fluid flow near the boundary slowing down the fluid motion. Figure 6 shows that the boundary layer thickness increases as the unsteadiness parameter increases. The velocity profiles decrease with increasing value of A.

Figure 7 shows that as β increases, the boundary layer thickness increases with a cross-over of profiles near the surface. The physical interpretation of this behavior is that an increase in β reduces the fluid in the flow leading to the boundary layer thickness increasing near the surface but a contrary trend is recognized away from the surface.

Figure 8 shows a reduction in the velocity with an increase in the mass suction parameter s. Figure 9 demonstrates the effect of A on the temperature profile. An increase in unsteadiness causes an increase in the solute concentration. Figure 10 shows how the temperature pro-

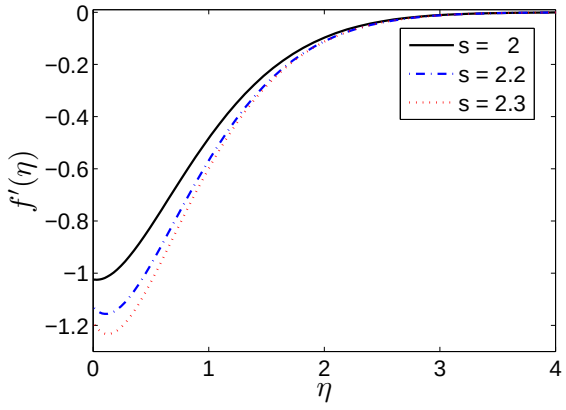

Figure 8: Effect of s on the velocity profile $f'(\eta)$

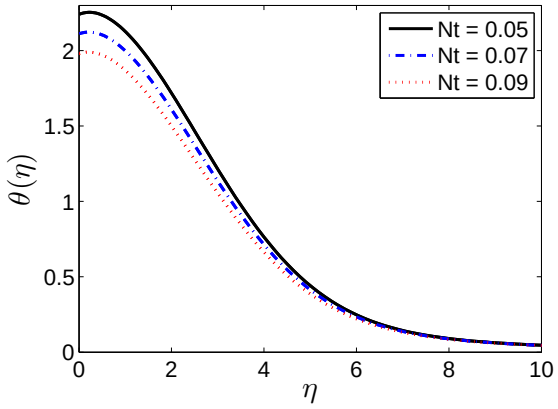

Figure 11: Effect of Nt on the temperature profile $\theta(\eta)$

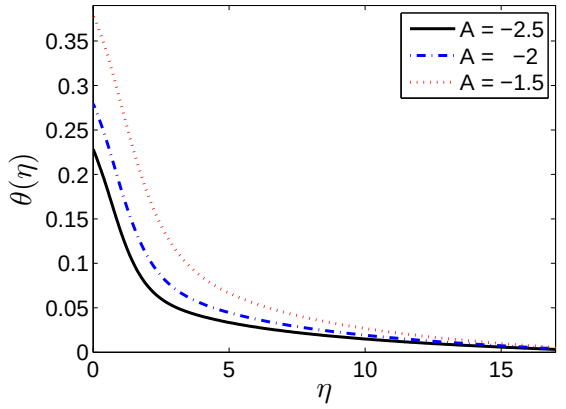

Figure 9: Effect of A on the temperature profile $\theta(\eta)$

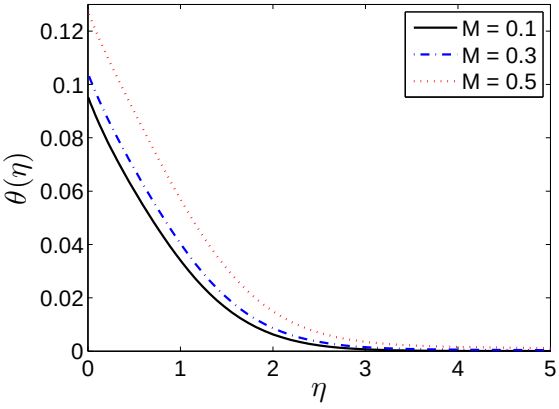

Figure 12: Effect of M on the temperature profile $\theta(\eta)$

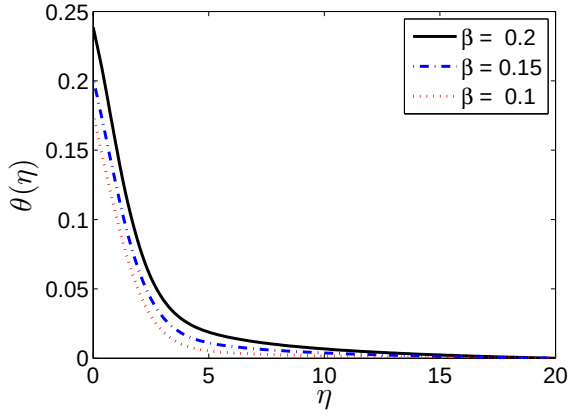

Figure 10: Effect of β on the temperature profile $\theta(\eta)$

files change with respect to variations in the Maxwell parameter β. The temperature profiles increase with increasing β values. This is to be expected since higher Maxwell parameters generally suggest a more solid material able to conduct and retain heat better.

Figure 11 shows the change in temperature profiles with respect to variations in the thermophoresis parameter values. As thermophoresis increases, the temperature profiles decrease near the surface. Figure 12 shows the effect of the magnetic field parameter on $\theta(\eta)$ the temperature profiles. We observe that the temperature profiles increase with increasing values of the magnetic field parameter. The existence of a magnetic field in an electrically conducting fluid produces a body force that decelerates the fluid flow which in turn has the effect of retaining more heat within the boundary layer.

The impact of the unsteadiness parameter, Maxwell parameter, Brownian motion parameter, thermophoresis parameter and the Schmidt number on the concentration profiles is depicted in Figures 13 - 16. In Figures 13 and 14

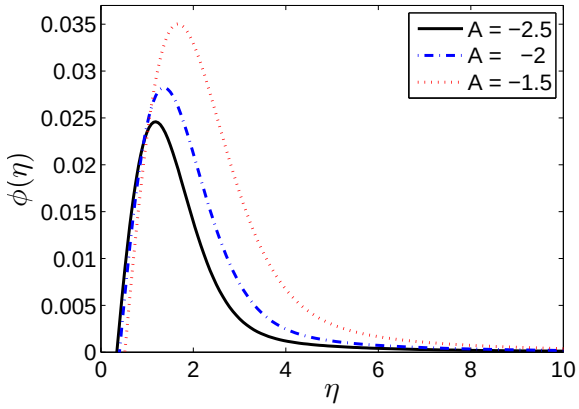

Figure 13: Effect of unsteadiness parameter A on the concentration profile $\phi(\eta)$

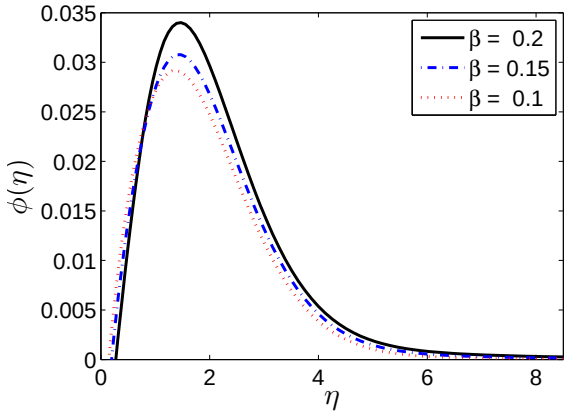

Figure 14: Effect of β on the concentration profile $\phi(\eta)$

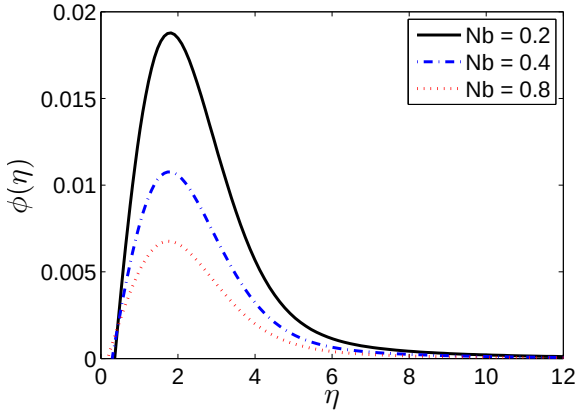

Figure 15: Effect of Nb on the concentration profile $\phi(\eta)$

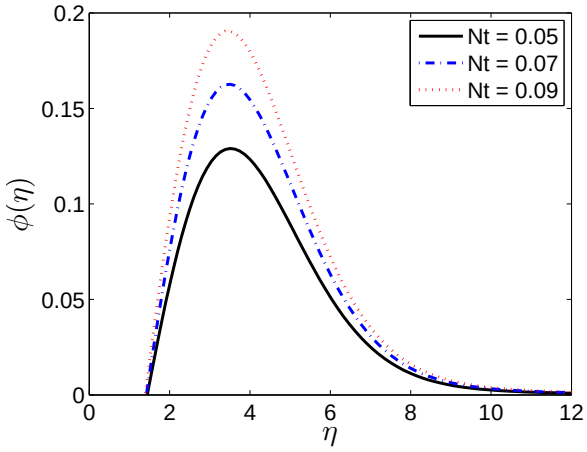

Figure 16: Effect of Nt on the concentration profile $\phi(\eta)$

an increase in the unsteadiness parameter and Maxwell parameter causes an increase in the concentration profiles near the surface but the opposite movement is observed far from the surface. Figure 15 shows the impact that the Brownian motion parameter has on the concentration profiles. An increase in the Brownian motion parameter causes a decrease in the concentration profiles. The Brownian motion tends to intensify particle displacement away from the fluid flow regime onto the surface; this phenomenon accounts for a decrease in the concentration of the nanoparticles far from the surface, thus resulting in a decrease in the nanoparticle concentration boundary layer thickness.

Figure 16 depicts the effect of the thermophoresis parameter on the concentration profiles. Thermophoresis is associated with the movement of nanoparticles from a hot to a cold wall, and since it is generated by temperature gradients, this creates a fast flow away from the moving surface. Consequently more fluid is heated away from the surface leading to an increase in the temperature within the thermal boundary layer.

5 Conclusion

In this study, we have investigated unsteady Maxwell nanofluid flow over a shrinking sheet with convective and slip boundary conditions. The conservation equations were solved using an iterative spectral local linearization method. We have given an error analysis to establish the accuracy and convergence of the method. The impact and significance of various physical parameters on the fluid properties has been demonstrated both qualitatively and

quantitatively. The findings can be briefly outlined as follows;

1. The concentration and velocity profiles decrease whereas the temperature profile increases with increasing unsteadiness parameter.
2. Increasing particle Brownian motion leads to a reduction in the concentration profiles but concentration profiles increase with increasing thermophoresis.
3. In terms of heat transfer coefficients, increasing value of particle Brownian motion and magnetic field strength reduces the heat transfer coefficient but the opposite is observed in the case of increased thermophoresis parameter.

Acknowledgement: The authors are grateful to the University of KwaZulu-Natal and the Claude Leon Foundation, South Africa for financial support.

Conflict of Interests: The authors declare that there is no conflict of interests regarding the publication of this article.

References

[1] Mushtaq A., Abbasbandy S., Mustafa M., Hayat T., Alsaedi A., et al., Numerical solution for Sakiadis flow of upper-convected Maxwell fluid using Cattaneo-Christov heat flux model, AIP Adv., 2016, 6, 015208.

[2] Sochi T., Flow of non-Newtonian fluids in porous media, J. Polym. Sci. B Polym. Phys., 2010, 48,2437–2767.

[3] Gallegos C., Martínez-Boza F.J., Linear viscoelasticity. Rheology: encyclopedia of life support systems (EOLSS), UNESCO, Eolss, Oxford, 2010, 120–143.

[4] Choi J.J., Rusak Z., Tichy J.A., et al., Maxwell fluid suction flow in a channel, J. Non-Newtonian Fluid Mech., 1999, 85, 165–187.

[5] Nandy S.K., Unsteady flow of Maxwell fluid in the presence of nanoparticles toward a permeable shrinking surface with Navier slip, J. Taiwan Inst. Chem. Eng., 2015, 52, 22–30.

[6] Rashidi M.M., Rostami B., Freidoonimehr N., Abbasbandy S., et al., Free convective heat and mass transfer for MHD fluid flow over a permeable vertical stretching sheet in the presence of the radiation and buoyancy effects, Ain Shams Eng. J., 2014, 5, 901–912.

[7] Awais M., Hayat T., Irum S., Alsaedi A., et al., Heat generation/absorption effects in a boundary layer stretched flow of Maxwell nano fluid: Analytic and numeric solutions, PloS one, 2015, 10, e0129814.

[8] Choi S.U.S., Eastman J.A., Enhancing thermal conductivity of fluids with nanoparticles, ASME, International Mechanical Engineering Congress and Exposition, San Francisco, CA, November 12-17, 1995.

[9] Yu W., France D.M., Routbort J.L., Choi S.U.S., et al., Review and comparison of nano fluid thermal conductivity and heat transfer enhancements, Heat Transfer Eng. 2008, 29, 432–460.

[10] Mukhopadhyay S., Bhattacharyya K., Unsteady flow of a Maxwell fluid over a stretching surface in presence of chemical reaction, J. Egyptian Math. Soc., 2012, 20, 229–234.

[11] Nandy S.K., Sidui S., Mahapatra T.R., et al., Unsteady MHD boundary layer flow and heat transfer of nano fluid over a permeable shrinking sheet in the presence of thermal radiation, Alex. Eng. J., 2014, 53, 929–937.

[12] Das K., Duari P.R., Kundu P.K., et al., Numerical simulation of nano fluid flow with convective boundary condition, J. Egyptian Math. Soc., 2015, 23, 435–439.

[13] Hayat T., Shafiq A., Alsaedi A., Asghar S., et al., Effect of inclined magnetic field in flow of third grade fluid with variable thermal conductivity, AIP Adv., 2015, 5, 087108.

[14] Hayat T., Shehzad S.A., Qasim M., Alsaedi A., et al., Mixed convection flow by a porous sheet with variable thermal conductivity and convective boundary condition, Braz. J. Chem. Eng., 2014, 31, 109–117.

[15] Hayat T., Qasim M., Effects of thermal radiation on unsteady magneto hydrodynamic flow of a micropolar fluid with heat and mass transfer, Z. Naturforsch. A, 2010, 65, 950–960.

[16] Hayat T., Qasim M., Influence of thermal radiation and Joule heating on MHD flow of a Maxwell fluid in the presence of thermo phoresis,Int. J. Heat Mass Trans., 2010, 53, 4780–4788.

[17] Som N.M., Md Arifin N., Md Ali F., Nazar R., et al., Non-darcy flow and heat transfer over a permeable stretching sheet embedded in a porous media with thermal radiation and Ohmic dissipation, Int. J. Theor. Appl. Mech., 2016, 1, 13–18.

[18] Hsiao K.L., Conjugate heat transfer for mixed convection and Maxwell fluid on a stagnation point, Arab. J. Sci. Eng.,2014, 39, 4325–4332.

[19] Mahapatra, T.R., Mondal S., Pal D., et al., Heat transfer due to magneto hydrodynamic stagnation-point flow of a power-law fluid towards a stretching surface in the presence of thermal radiation and suction/injection, ISRN Thermodynamics, 2012, 2012, 1–9.

[20] Motsa S.S., A new spectral local linearization method for nonlinear boundary layer flow problems, J. Appl. Math., 2013, 2013, 1–15.

[21] Motsa S.S., Makukula Z.G., Shateyi S., et al., Spectral local linearisation approach for natural convection boundary layer flow, Math. Prob. Eng., 2013, 2013, 1–7.

[22] Buongiorno J., Convective transport in nano fluids, J. Heat Trans., 2006,128, 240–250.

[23] Shateyi S., Marewo G.T., On a new numerical analysis of the hall effect on MHD flow and heat transfer over an unsteady stretching permeable surface in the presence of thermal radiation and heat source/sink, Boundary Value Prob., 2014, 2014, 1–17.

[24] Hayat T., Shehzad S.A., Qasim M., Obaidat S., et al., Steady flow of Maxwell fluid with convective boundary conditions, Z. Naturforsch. A, 2011, 66, 417–422.